JOURNAL OF AIRCRAFT
Vol. 45, No. 4, July–August 2008

Eulerian Modeling of In-Flight Icing Due to Supercooled Large Droplets

Raimund Honsek* and Wagdi G. Habashi†
McGill University, Montreal, Quebec, H3A 2S6, Canada
and
Martin S. Aubé‡
Newmerical Technologies International, Montreal, Quebec, H3A 2M7, Canada

DOI: 10.2514/1.34541

To accurately simulate the impingement behavior and associated icing potential of supercooled large droplets, droplet–wall interactions including splashing and bouncing phenomena must be accounted for in the governing Eulerian model. Because of current limitations in computational capacity, an industrially viable simulation is necessarily based on a semi-empirical description of the droplet–wall interaction process. Because empirical correlations are inherently Lagrangian in nature, the associated information must be transformed from a Lagrangian to an Eulerian frame of reference. A detailed derivation of an Eulerian model of the droplet–wall interaction process is presented, along with a comparison of numerical and experimental collection efficiency distributions demonstrating the model's current simulation capabilities.

Nomenclature

a	=	air
C_D	=	drag coefficient
d	=	droplet, when used as a subscript
d	=	droplet diameter, μm
$\boldsymbol{F}_S$	=	splashing or bouncing force, N
Fr	=	Froude number
Ga	=	Galileo number
$\hat{g}$	=	gravitational unit vector, −
K	=	inertial parameter
K_C	=	Cossali parameter
La	=	Laplace number
n	=	normal
o	=	preimpact, prebreakup
R	=	roughness parameter, $R = r/d_o$
Re_d	=	droplet Reynolds number
Re_t	=	terminal Reynolds number
r	=	surface roughness, μm
s	=	postimpact, postbreakup
stab	=	stable
t	=	tangential
$\boldsymbol{U}_\infty$	=	freestream velocity, m/s
$\boldsymbol{u}_a$	=	normalized air velocity, −
$\boldsymbol{u}_d$	=	normalized droplet velocity, −
$\boldsymbol{u}_t$	=	normalized terminal velocity, −
We_b	=	breakup Weber number
We_s	=	impact Weber number
α	=	normalized volume fraction, −
β	=	collection efficiency, −
ΔT_S	=	collision contact time, −
θ	=	incidence angle, deg
μ	=	dynamic viscosity, Pa · s
ρ	=	density, kg/m^3
σ	=	surface tension, N/m
∞	=	freestream
0	=	initial

Presented as Paper 465 at the 44th AIAA Aerospace Sciences Meeting and Exhibit, Reno, Nevada, 9–12 January 2006; received 11 September 2007; accepted for publication 9 January 2008.

*Masters Student, Computational Fluid Dynamics Laboratory, Department of Mechanical Engineering, 688 Sherbrooke Street West; currently with Exxon Research, Calgary, Alberta, Canada.

†Professor and NSERC-J. Armand Bombardier Industrial Research Chair of Multidisciplinary CFD, Computational Fluid Dynamics Laboratory, Department of Mechanical Engineering, 688 Sherbrooke Street West. Associate Fellow AIAA.

‡Vice President Operations, 680 Sherbrooke Street West.

I. Introduction

AIRCRAFT lift and control surfaces exposed to meteorological conditions featuring liquid water content (LWC) in the form of supercooled droplets at temperatures below the freezing point are subject to ice accretion and an inherent deterioration of aerodynamic performance characteristics. Traditionally, the design of antiicing measures is based on the impingement limits corresponding to droplet size distributions featuring mean volumetric diameters (MVD) of 40 μm or less, as currently defined in Appendix C of the Federal Aviation Regulation (FAR) 25 regulations. However, a renewed focus on meteorological research conducted in response to the icing-induced loss of control and subsequent crash of an ATR-72 commuter aircraft near Roselawn, Indiana, on 31 October 1994 has confirmed the existence of supercooled large droplets (SLD) featuring MVDs up to 400 μm. Ice accretions due to SLD may result in extremely severe aircraft performance degradation, including a reduction in stall angle accompanied by an increase in stall speed, a reduction in lift in excess of 60%, and an increase in drag up to 200%. Because of the large size and inherently ballistic trajectories of SLD droplets, the corresponding ice accretions may be established downstream of the impingement regions protected by antiicing measures leading to a potentially uncontrolled ice-accretion process [1,2].

Clearly, the design of antiicing measures based on the current maximum MVD of 40 μm is insufficient, and an extension of numerical simulation techniques to include SLD droplet impingement is required. Although principally feasible, such an extension is complicated by the fact that droplets in the SLD regime violate fundamental assumptions regarding the impingement behavior of droplets within the envelope of Appendix C regulations. The most important of these violations pertain to the following simplifying assumptions originally made by Bourgault et al. [3] in the derivation of the mathematical equations governing droplet behavior:

1) Droplets travel at the freestream velocity relative to the approaching aircraft.

2) Droplets do not deform or break up due to aerodynamic shear in the vicinity of the aircraft.

3) Droplets do not coalesce, bounce, or splash upon impact on the aircraft.

Because of their large MVD, SLD droplets no longer enjoy a stable atmospheric stratification but much rather resemble a droplet cloud falling at terminal velocity. Hence, an additional vectorial component is introduced in the droplet's initial approach velocity, resulting in an altered impingement trajectory. Another effect of large droplet MVDs is a tendency for droplets to deform under the influence of aerodynamic shear forces, resulting in increased aerodynamic drag. The effect of aerodynamic shear may become sufficiently manifested in the vicinity of aircraft surfaces to cause eventual droplet breakup, resulting in a reduction of the droplet distribution's MVD before impingement. Both of these effects result in a more pronounced aerodynamic influence on droplet trajectories [4,5].

Depending on impingement surface conditions such as roughness and film height as well as an approaching droplet's kinetic energy, a droplet–wall collision may result in the complete or partial deposition of the impinging droplet mass. For the case of droplet distributions featuring an MVD within the Appendix C envelope, an approaching droplet's kinetic energy is sufficiently low to justify the assumption of negligible bouncing and splashing effects. However, empirical as well as computational studies have convincingly demonstrated the occurrence of droplet splash and rebound phenomena for droplet size distributions beyond the Appendix C limit. Under such circumstances, the approaching droplet mass is only partially deposited at the predicted impingement location while the splashed or rebounded mass fraction is reintroduced into the flow field, potentially resulting in reimpingement on aircraft lift and control surfaces located downstream of actively protected regions [6,7].

To address the shortcomings of current numerical simulation capabilities within the SLD regime of droplet impingement, the necessary extensions of an existing three-dimensional Eulerian droplet impingement code, DROP3D [3,8–10], will be presented in this paper. The original mathematical model will be briefly presented, followed by select results of a review of published literature pertaining to empirical descriptions of droplet–wall interactions so as to establish a suitable context for the detailed derivation of a proposed mathematical model of droplet–wall interactions in an Eulerian frame of reference.

II. Original Mathematical Model

In contrast to the Lagrangian formulation employed by the ONERA [11] and NASA LEWICE [12] droplet impingement codes, DROP3D relies on a purely Eulerian model. The simulation of the impingement process by a Lagrangian approach introduces a numerical technique fundamentally different from the Eulerian formulation of the aerodynamic field solver, potentially resulting in the need for multiple grids. An Eulerian formulation, on the contrary, treats the dispersed liquid phase as a continuum; this enables the prediction of droplet volume fractions and velocity components at the same nodes as the aerodynamic solution and avoids the interpolation intensive particle tracking process of the Lagrangian formulation.

A. Governing Equations

The particular Eulerian formulation of the droplet impingement process employed by DROP3D yields a set of partial differential equations representing the continuity equation (1) and momentum equations (2) of the dispersed droplet phase, as presented previously by Bourgault et al. [3]:

$$\frac{\partial \alpha}{\partial t} + \boldsymbol{u}_d \cdot \nabla \alpha + \nabla \cdot \boldsymbol{u}_d = 0 \tag{1}$$

$$\frac{D\boldsymbol{u}_d}{Dt} = \frac{\partial \boldsymbol{u}_d}{\partial t} + \boldsymbol{u}_d \cdot \nabla \boldsymbol{u}_d = \frac{C_D Re_d}{24K}(\boldsymbol{u}_a - \boldsymbol{u}_d) + \left(1 - \frac{\rho_a}{\rho_d}\right)\frac{\hat{g}}{Fr^2} \tag{2}$$

The droplet momentum equations (2) are expressed in nonconservative form and is formulated based on the assumption that a droplet in motion is only subject to aerodynamic drag, buoyancy, and gravity forces.

B. Boundary Conditions

A detailed analysis of system characteristics performed by Bourgault et al. [3] reveals that Dirichlet boundary conditions are required for both droplet volume fraction and velocity at the inflow boundary of the computational domain. Specification of boundary conditions at solid boundaries or outflow boundaries of the computational domain is neither required nor permissible to uniquely determine the solution of the governing equations. A suitable initial solution respecting these boundary condition requirements is to set $\alpha = 1$ and $\boldsymbol{u}_d = [\cos(AoA), \sin(AoA), 0]$ throughout the computational domain. An exception applies to locations within the immediate vicinity of solid boundaries in which both the droplet volume fraction and velocity are initially set to zero.

III. Literature Findings

To accurately simulate droplet impingement behavior in the SLD regime, the original mathematical model must be extended to include the effects of terminal droplet velocity, droplet deformation and breakup, as well as droplet–wall interactions on droplet trajectories in the vicinity of aircraft surfaces. Select results of a detailed review of published literature pertaining to dispersed liquid-gas flows and droplet–wall interactions reported in a variety of engineering applications will be presented to justify the adopted mathematical formulation.

A. Terminal Droplet Velocity

As the droplet velocity appears in both the drag coefficient and the droplet Reynolds number, there is a general difficulty in establishing correlations expressing a droplet's terminal velocity in terms of the corresponding Reynolds number. Hence, a dimensionless group known as the Galileo number may be defined as a function of physical properties of the gas and liquid phase to eliminate the unknown terminal velocity. Khan and Richardson [13] derive a comprehensive correlation expressing the Reynolds number as a function of the Galileo number over the range of $1.0e-2 \leq Re_t \leq 3.0e+5$:

$$Re_t = (2.33Ga^{0.018} - 1.53Ga^{-0.016})^{13.3} \tag{3}$$

Once the Reynolds number is evaluated, the corresponding terminal velocity may be obtained from the definition of the terminal Reynolds number:

$$\boldsymbol{u}_t = \frac{\mu_a}{\rho_a d U_\infty}(2.33Ga^{0.018} - 1.53Ga^{-0.016})^{13.3} \tag{4}$$

B. Droplet Deformation and Breakup

Droplets featuring a large diameter are prone to deformation under the influence of aerodynamic shear forces, resulting in a decidedly nonspherical shape. Clift et al. [14] propose an extended drag model based on droplet eccentricity and vibrational distortion to account for the associated increase in aerodynamic drag at SLD conditions:

$$C_D = \begin{Bmatrix} (1.0-f)C'_D + fC''_D & We_b \leq 12 \\ C'_D & We_b > 12 \end{Bmatrix} \tag{5}$$

The eccentricity function f is defined as a function of the breakup Weber number:

$$f = 1.0 - (1.0 + 0.07\sqrt{We_b})^{-6} \tag{6}$$

The parameters C'_D and C''_D represent the drag coefficients of an oblate disk and a spherical particle, respectively. Hence, the effective drag coefficient defined by Eq. (5) will approach that of a spherical particle at low Weber numbers while tending toward that of an oblate disk at elevated Weber numbers.

Droplets may experience vibrational distortion eventually leading to acceleration-induced breakup under the influence of sufficiently pronounced aerodynamic shear. Pilch and Erdman [15] identify five distinct breakup mechanisms, characterized by the initial droplet Weber number and the associated nondimensional breakup time T as follows:

$$T = \begin{Bmatrix} 6.000(We_b - 12)^{-0.25} & 1.2e+1 \le We_b \le 1.8e+1 \\ 2.450(We_b - 12)^{+0.25} & 1.8e+1 \le We_b \le 4.5e+1 \\ 14.10(We_b - 12)^{-0.25} & 4.5e+1 \le We_b \le 3.5e+2 \\ 0.766(We_b - 12)^{+0.25} & 3.5e+2 \le We_b \le 2.7e+3 \\ 5.500 & 2.7e+3 \le We_b \end{Bmatrix} \tag{7}$$

Based on the assumption that postbreakup droplet fragments eventually acquire subcritical Weber numbers, the maximum stable droplet diameter at cessation of all breakup activities is based on the definition of the critical droplet breakup Weber number:

$$We_{b,\text{crit}} = 12 \Rightarrow d_{\text{stab}} = \frac{12\sigma}{\rho_a U_\infty^2 |\boldsymbol{u}_a - \boldsymbol{u}_d|^2} \tag{8}$$

C. Droplet–Wall Interactions

Bai and Gosman [16] identify four possible mechanisms of droplet–wall interactions within the operational envelope of in-flight icing, including the stick, rebound, spread, and splash mechanisms illustrated schematically in Fig. 1:

1) Stick: At sufficiently low impact velocities and surface temperatures, the impinging droplet sticks to the impact surface in approximately spherical form.

2) Rebound: At low impact velocities a film of air may be entrained between the impinging droplet and a wetted impact surface, causing the droplet to rebound off the surface following impact.

3) Spread: At moderate impact velocities, the impinging droplet ruptures and forms a liquid film on a dry impact surface or coalesces with the existing film on a wetted impact surface.

4) Splash: At sufficiently high impact velocities, the impinging droplet disintegrates and a liquid sheet is ejected from the impact surface, leading to the formation of droplet fragments along its periphery.

Because of current limitations in computational capacity, an industrially viable model of droplet–wall interactions must be based on a semi-empirical formulation of the impingement process. As merely the stick and spread mechanisms are accounted for in the original mathematical formulation of DROP3D, semi-empirical descriptions are required for the rebound and splashing mechanisms. To enable an unambiguous definition, Fig. 2 illustrates pertinent model parameters within the context of a typical collision.

A detailed review of published literature pertaining to droplet–wall collisions reveals a variety of semi-empirical modeling approaches. Following a critical appraisal of these models with respect to physical comprehensiveness and applicability in SLD conditions, the droplet impingement model proposed by Trujillo et al. [17] is deemed most suitable for the description of droplet splashing phenomena, whereas the model developed by Bai and Gosman [16] is considered to entail the most representative description of droplet bouncing processes. The distinction between droplet bouncing (R_1) and spreading regimes is based on a critical range of Weber numbers proposed by Bai and Gosman [16], whereas the transition between spreading and splashing (R_2) regimes is based on a critical value of the Cossali parameter identified by Trujillo et al. [17]:

$$\begin{Bmatrix} R_1 \\ R_2 \end{Bmatrix} \equiv \begin{Bmatrix} 10 \le We_{s,c} \le 1320La^{-0.18} \\ K_C \ge 540R^{-0.35} \end{Bmatrix} \tag{9}$$

Bai and Gosman [16] adopt the equations of motion pertaining to a solid particle rebounding off a solid surface:

$$\frac{u_{t,s}}{u_{t,o}} = \frac{5}{7} \tag{10}$$

$$\frac{u_{n,s}}{u_{n,o}} = -[0.9930 - 0.0307(90\ \text{deg} - \theta_o) + 0.0272(90\ \text{deg} - \theta_o)^2 - 0.0086(90\ \text{deg} - \theta_o)^3] \tag{11}$$

Trujillo et al. [17] determine expressions for the normal and tangential components of secondary droplet velocities from cumulative probability density functions based on the experimental data reported by Mundo et al. [18], whose mean values follow a simple functional relationship with the angle of incidence:

$$\frac{u_{t,s}}{u_{t,o}} = +(0.85 + 0.0025\theta_o) \tag{12}$$

$$\frac{u_{n,s}}{u_{n,o}} = -(0.12 + 0.0020\theta_o) \tag{13}$$

The number of secondary droplet fragments is obtained from experimental data reported by Stow and Stainer [19]:

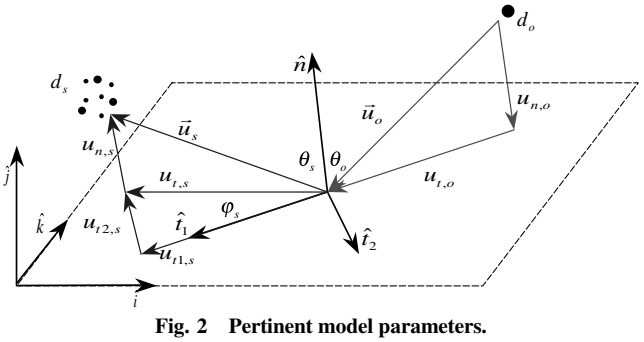

Fig. 2 Pertinent model parameters.

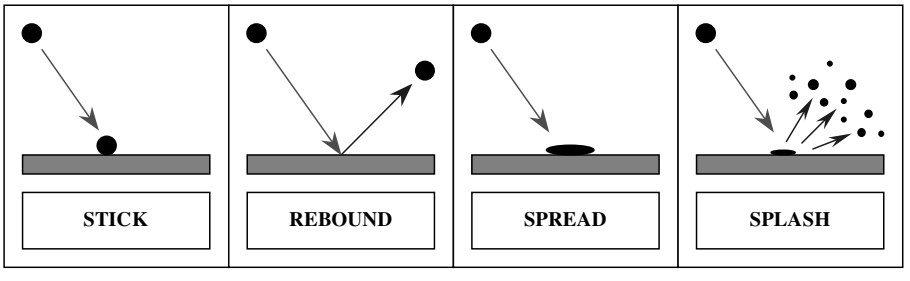

Fig. 1 Schematic representation of pertinent droplet–wall interaction mechanisms.

$$N_s = \frac{1}{22}\left\{0.0437\left[K_C\left(\frac{|\boldsymbol{u}_o|}{u_{n,o}}\right)^2 - K_{C,\mathrm{dry}}\right] - 44.92\right\} \tag{14}$$

The splashed-to-incident droplet mass ratio is based on the experimental data reported by Yarin and Weiss [20]:

$$\frac{m_s}{m_o} = 0.8[1.0 - e^{-0.85(K'_Y - 17)}] \tag{15}$$

Finally, secondary droplet diameters may be determined from the total number and mass of secondary droplets combined with the principle of mass conservation:

$$\frac{d_s}{d_o} = \left(\frac{m_s}{m_o}\frac{1}{N_s}\right)^{\frac{1}{3}} \tag{16}$$

The experimental range of incident droplet diameters [25 μm $\leq d_o \leq$ 880 μm] and velocities [0 m/s $\leq |\boldsymbol{u}_o| \leq$ 43 m/s] justifies the application of this particular empirical model in SLD conditions.

IV. Extended Mathematical Model

A. Terminal Droplet Velocity

Once the terminal velocity corresponding to a given droplet diameter is obtained from Eqs. (3) and (4), the initial conditions may be changed accordingly:

$$\boldsymbol{u}_d = \begin{Bmatrix} u_d \\ v_d \\ w_d \end{Bmatrix} = \begin{Bmatrix} u_{d-t} + g_x|\boldsymbol{u}_t| \\ v_{d-t} + g_y|\boldsymbol{u}_t| \\ w_{d-t} + g_z|\boldsymbol{u}_t| \end{Bmatrix} \tag{17}$$

In Eq. (17), $\{u_{d-t}, v_{d-t}, w_{d-t}\}$ denotes the initial droplet velocity vector in the absence of the terminal droplet velocity while $\{g_x, g_y, g_z\}$ represents the gravitational unit vector in the global Cartesian coordinate system.

B. Droplet Deformation and Breakup

The evolution of the local droplet diameter under the influence of droplet breakup due to aerodynamic shear is governed by the following partial differential equation as proposed by Lodej [21]:

$$\frac{Dd}{Dt} = \frac{\partial d}{\partial t} + \boldsymbol{u}_d \cdot \nabla d = \frac{d_{\mathrm{stab}} - d_o}{T} \tag{18}$$

Equation (18) models the evolution in time of the droplet diameter, which tends to a stable diameter d_{stab}, given by Eq. (8), after a characteristic time T Eq (7). The source term represents the speed at which the droplet reaches a stable diameter.

C. Droplet–Wall Interactions

Although limited in computational elegance, the Lagrangian formulation lends itself well to the description of droplet–wall interaction processes. Droplet trajectories may be developed throughout the computational domain until a solid boundary is encountered. Subsequently, secondary droplet sizes and velocity components obtained from empirical correlations may be imposed as initial conditions for further time integration of droplet trajectories. However, as the notion of individual droplets does not exist in an Eulerian formulation, an adequate mathematical description of the physical phenomena observed during droplet–wall collisions is not easily conceived.

A formulation of the droplet–wall interaction process in terms of a body force applicable at solid boundaries facilitates a straightforward extension of the method used to derive the original droplet momentum equations:

$$\frac{D\boldsymbol{u}_d}{Dt} = \frac{\partial \boldsymbol{u}_d}{\partial t} + \boldsymbol{u}_d \cdot \nabla \boldsymbol{u}_d = \frac{1}{m_o}[\boldsymbol{F}_D + \boldsymbol{F}_B + \boldsymbol{F}_G + \boldsymbol{F}_S] \tag{19}$$

where $\boldsymbol{F}_D$, $\boldsymbol{F}_B$, and $\boldsymbol{F}_G$ represent, respectively, the air drag, buoyancy, and gravity forces of Eq. (2). $\boldsymbol{F}_S$, the change of momentum due to splashing, will be defined in this section.

The original droplet momentum equations (2) suffice to model the stick and spread mechanisms insofar as droplet trajectories terminate at solid boundaries following impact. Therefore, the body force associated with the change in droplet momentum due to impingement phenomena merely needs to account for the effects of droplet bouncing and splashing. The corresponding body force should be based on the momentum change introduced by the translation of secondary droplet mass following impingement:

$$\boldsymbol{F}_S = \left.\frac{d(m_d\boldsymbol{u}_d)}{dt}\right|_S = m_s \left.\frac{d\boldsymbol{u}_d}{dt}\right|_S \tag{20}$$

Strictly speaking, the time derivative in Eq. (20) represents the instantaneous change in momentum incurred by the secondary droplet mass at the time of impact due to the impulse delivered by the target surface. To the knowledge of the authors, however, the published literature reveals no information regarding the magnitude of such an impulse. The proposed formulation hence approximates the exact time derivative by a linear variation between pre- and postimpact velocities over an associated collision contact time interval:

$$\boldsymbol{F}_S \approx m_s \left.\frac{\Delta \boldsymbol{u}_d}{\Delta t}\right|_S = m_s\left(\frac{\boldsymbol{u}_s - \boldsymbol{u}_o}{\Delta T_S}\right) \tag{21}$$

Within the context of Eq. (21), the contact time may be considered as the time span required for a droplet to decelerate from its initial impingement velocity upon approaching a surface, come to a temporary rest on the surface, and accelerate to the postimpact velocity predicted by the applicable empirical description. To accommodate the functionality of the chosen empirical correlations, a recast of Eq. (21) is necessary:

$$\begin{aligned}\boldsymbol{F}_S &= m_o\left(\frac{m_s}{m_o}\right)\left\lfloor \frac{\boldsymbol{u}_o}{\Delta T_S}\left(\frac{\boldsymbol{u}_s}{\boldsymbol{u}_o} - 1\right)\right\rfloor = \frac{m_o\boldsymbol{u}_o}{\Delta T_S}\left(\frac{m_s}{m_o}\right)\left(\frac{\boldsymbol{u}_s}{\boldsymbol{u}_o} - 1\right) \\ &= \frac{m_o\boldsymbol{u}_o}{\Delta T_S} f_m(f_u - 1)\end{aligned} \tag{22}$$

The functions f_m and f_u have been initially adopted from Bai and Gosman [16] as well as Trujillo et al. [17], and subsequently calibrated against SLD specific droplet impingement data provided by Papadakis et al. [22]:

$$f_m = \frac{m_s}{m_o} = \begin{Bmatrix} 1.0 & R_1 \\ 3.8[1.0 - e^{-0.85(K'_Y - 17)}]/[K'_Y]^{0.5} & R_2 \end{Bmatrix} \tag{23}$$

$$f_{u,t} = \frac{u_{t,s}}{u_{t,o}} = + \begin{Bmatrix} 0.8500 + 0.0025\theta_o & R_1 \\ 0.8500 + 0.0025\theta_o & R_2 \end{Bmatrix} \tag{24}$$

$$\begin{aligned} f_{u,n} &= \frac{u_{n,s}}{u_{n,o}} \\ &= -\begin{Bmatrix} 0.9930 - 0.0307\bar{\theta}_o + 0.0272\bar{\theta}_o^2 - 0.0086\bar{\theta}_o^3 & R_1 \\ 0.1200 + 0.0020\theta_o & R_2 \end{Bmatrix} \end{aligned} \tag{25}$$

Okumura et al. [23] suggest an empirical correlation for the variation of the collision contact time with droplet diameter, whose functionality has been calibrated against the experimental data provided by Papadakis et al. [22]:

$$\Delta T_S = K_T\left[\frac{\rho_d d_{\mathrm{ref}}^3}{8\sigma}\right]^{\frac{1}{2}}\left[\frac{d_{\mathrm{ref}}}{d_o}\right]^n \Rightarrow n = \begin{Bmatrix} 0.2 & d_{\min} \leq d_o < d_{\mathrm{ref}} \\ 0.0 & d_o \geq d_{\mathrm{ref}} \end{Bmatrix} \tag{26}$$

Hence, a set of droplet momentum equations is obtained in an Eulerian frame of reference, which account for the presence of droplet–wall interactions:

$$\frac{D\boldsymbol{u}_d}{Dt} = \frac{\partial \boldsymbol{u}_d}{\partial t} + \boldsymbol{u}_d \cdot \nabla \boldsymbol{u}_d = \frac{C_D Re_d}{24K}(\boldsymbol{u}_a - \boldsymbol{u}_d) + \left(1 - \frac{\rho_a}{\rho_d}\right)\frac{\hat{g}}{Fr^2} + \frac{\boldsymbol{u}_d f_m}{\Delta T_S}(f_u - 1) \tag{27}$$

The body force accounting for droplet–wall interactions is identically zero throughout the computational domain with the exception of computational nodes located on solid boundaries featuring impingement characteristics within the bouncing and splashing regimes defined by Eq. (9).

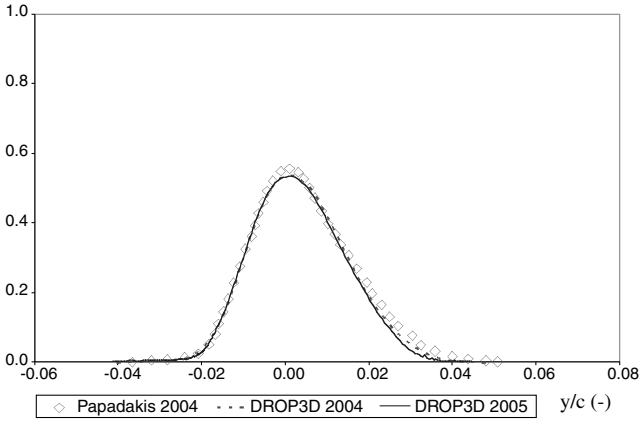

Fig. 3 Collection efficiency, MVD = 20 μm.

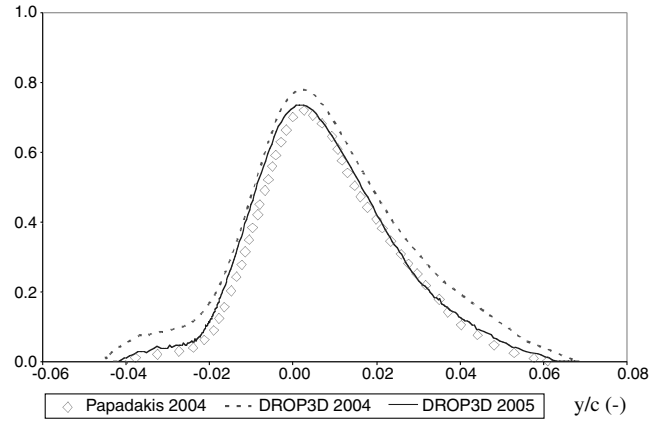

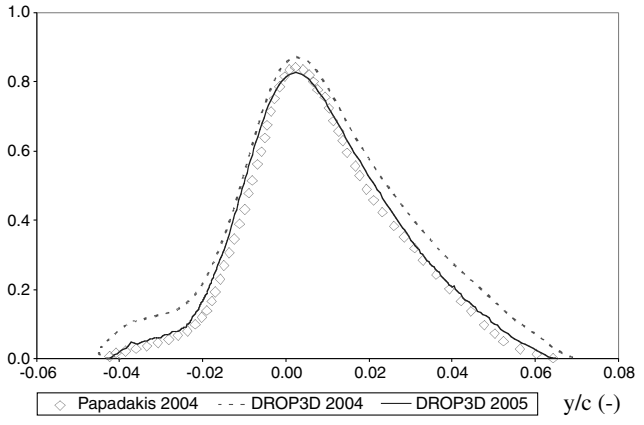

Fig. 4 Collection efficiency, MVD = 52 μm (left) and 111 μm (right).

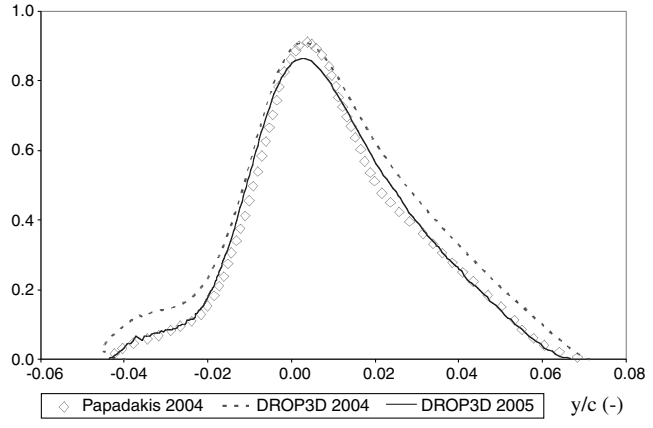

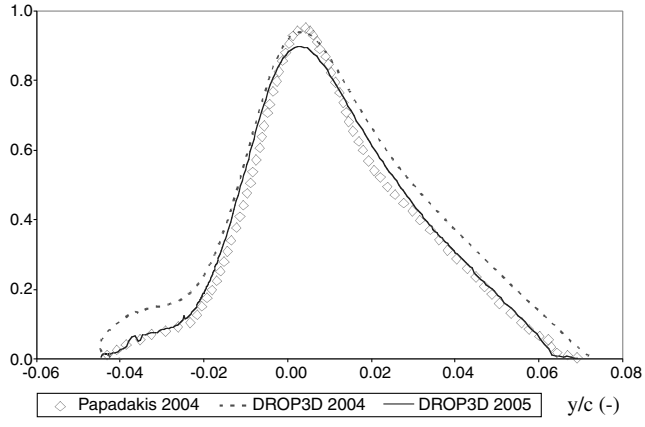

Fig. 5 Collection efficiency, MVD = 154 μm (left) and 236 μm (right).

V. Numerical Results

A nondimensional parameter of interest that quantifies a given location's ice-accretion potential is the local collection efficiency β, which represents the normalized influx of water at a surface and may be expressed in terms of the nondimensional droplet volume fraction and droplet velocity:

$$\beta = -\alpha \boldsymbol{u}_d \cdot \hat{n} \tag{28}$$

As the collection efficiency is a function of both droplet volume fraction and velocity and, hence, the droplet continuity and momentum equations, it facilitates a meaningful comparison of numerical and experimental results.

A. Model Calibration

The most comprehensive collection of experimental data pertaining to SLD specific droplet impingement originates from a recent study performed by Papadakis et al. [22] at NASA Glenn's Icing Research Tunnel. This detailed set of experimental data facilitates a systematic calibration of the functions f_m and f_u as well as the collision contact time over a large range of droplet diameters. The experimental test geometry consists of a NACA 23012 airfoil of 0.9144 m chord and 1.8288 m span, which is mounted vertically in a wind tunnel of 1.8288 m height and 2.7432 m width. The following aerodynamic boundary conditions characterize the mainstream flow:

1) freestream velocity: $U_\infty = 78.23$ m/s;
2) freestream temperature: $T_\infty = 299.00$ K;
3) freestream pressure: $p_\infty = 101.33$ kPa;
4) geometric angle of attack: $AoA = 2.50$ deg .

The experimental droplet size distributions featuring MVDs of 20, 52, 111, 154, and 236 μm are approximated using 27 droplet size groups. Figures 3–7 compare collection efficiency distributions

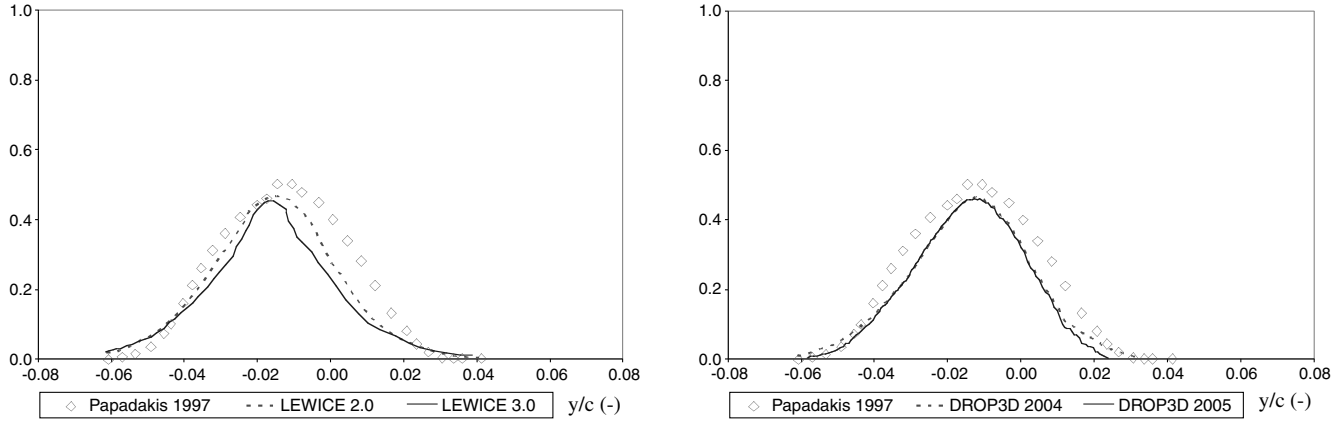

Fig. 6 Collection efficiency, MVD = 21 μm, LEWICE (left) and DROP3D (right).

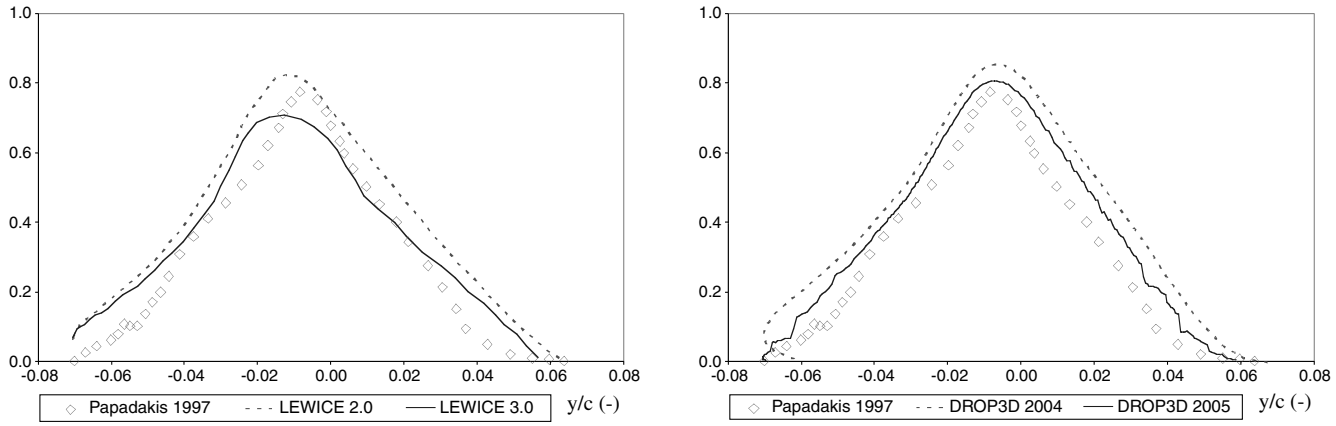

Fig. 7 Collection efficiency, MVD = 92 μm, LEWICE (left) and DROP3D (right).

based on the consideration of Eq. (27) rather than Eq. (2) in the proposed mathematical model, or DROP3D 2005 with numerical results based on the original mathematical model (DROP3D 2004) as well as experimental results (Papadakis 2004).

Excellent agreement between numerical and experimental collection efficiency distributions is observed throughout the droplet impingement region at MVDs of 20, 52, and 111 μm, whereas a deviation from experimental data within the vicinity of the airfoil leading edge becomes increasingly apparent at elevated MVDs of 154 μm and 236 μm. It should be noted that in some cases the maximum collection efficiency observed in the experiment exceeds the maximum collection efficiency obtained from numerical simulations in the absence of droplet–wall interactions. At this point it is unclear whether this discrepancy is attributable to the original mathematical model or a deficiency in the experimental measurement methods, which produce fluctuations in the value of the maximum collection efficiency by up to 10% as reported by Papadakis et al. [22]. In any case, it would appear sensible that the maximum collection efficiency obtained under consideration of droplet–wall interactions should not exceed the value obtained without the consideration of mass loss. As such, the proposed mathematical model may be considered mathematically consistent and physically representative. Considering the overall quality of the numerical results, the mathematical model of droplet–wall interactions may be deemed sufficiently calibrated.

B. Model Validation

To establish the model's applicability to arbitrary geometries, flow conditions, and droplet size distributions, it is validated against an unrelated set of experimental data. Because reliable data pertaining to SLD-specific droplet–wall interactions are rarely available at this point in time, the proposed mathematical formulation is validated against a set of data originating from a previous study performed by Papadakis et al. [24] at NASA Glenn's Icing Research Tunnel. The experimental test geometry consists of an MS317 airfoil of 0.9144 m chord and 1.8288 m span, which is mounted vertically in a wind tunnel of 1.8288-m height and 2.7432-m width. The following aerodynamic boundary conditions characterize the mainstream flow:

1) freestream velocity: $U_\infty = 78.68$ m/s;
2) freestream temperature: $T_\infty = 281.00$ K;
3) freestream pressure: $p_\infty = 94.67$ kPa;
4) geometric angle of attack: $AoA = 8.00$ deg.

The experimental droplet size distributions featuring MVDs of 21 and 92 μm are approximated using seven droplet size groups. The distributions of collection efficiencies obtained from the proposed mathematical model (DROP3D 2005) are compared with numerical results based on the original mathematical model (DROP3D 2004) as well as experimental data (Papadakis 1997). An additional comparison may be made to numerical results published in 2004 by Wright and Potapczuk [25] obtained from droplet impingement simulations based on NASA's LEWICE [12] code. Traditionally, LEWICE merely facilitates an estimate of droplet impingement characteristics in the absence of droplet–wall interactions (LEWICE 2.0). However, a recent adoption of the impingement model proposed by Trujillo et al. [17] considers the effects of droplet splashing, whereas the concept of droplet bouncing is not addressed by the extended mathematical model (LEWICE 3.0).

An inspection of Fig. 6 discloses the tendency of LEWICE to predict significant mass loss due to splashing near the airfoil leading edge, a surprising result for a droplet distribution featuring an MVD of 21 μm. DROP3D predicts negligible mass loss near the airfoil leading edge as expected, attributing only a slight amount of mass loss to droplets bouncing off the airfoil near the impingement limits. Hence, the proposed mathematical model predicts collection efficiency distributions in close agreement with experimental observations at an MVD of 21 μm, whereas numerical results obtained from LEWICE exhibit deviations from experimental reference data.

The pronounced differences regarding the location and extent of mass loss as predicted by LEWICE and DROP3D become more apparent in the simulation of larger droplet size distributions featuring an MVD of 92 μm, as illustrated in Fig. 7. Although the significant mass loss near the airfoil leading edge as predicted by LEWICE is physically justifiable and generally serves to improve the quality of the numerical results, the deviation from experimental reference data becomes increasingly pronounced as the impingement limits are approached. Wright and Potapczuk [25] attribute this deviation to a failure of the splashing model proposed by Trujillo et al. [17], associated with the pronounced decrease in the impingement velocity's magnitude observed in the limit of flow tangency. However, the droplet splashing model ceases to be applicable at such locations, and the deviation reported by Wright and Potapczuk [25] may be caused rather by the lack of a droplet bouncing model in the mathematical formulation of LEWICE. The collection efficiency distributions predicted by DROP3D support this conclusion, as a substantial amount of mass loss due to droplet bouncing is observed near the impingement limits, resulting in close agreement with experimental reference data.

VI. Conclusions

A suitable mathematical model for the description of droplet–wall interactions in an Eulerian frame of reference has been proposed and successfully calibrated against experimental reference data. The good agreement between numerical and experimental data observed for the calibration test case serves to demonstrate the proposed mathematical model's simulation capabilities as collection efficiencies and velocity profiles are predicted in close agreement with experimental observations.

The deviations from experimental data observed in the simulation of the validation test case may be attributable either to an insufficiently (only one test case) broad calibration of the proposed mathematical model or to a deficiency in experimental measurement methods. A need for extensive comparison with experimental data may thus be identified to verify whether the currently proposed expressions governing collision contact time and splashed mass fraction are indeed applicable to arbitrary geometries and flow conditions. However, reliable experimental data pertaining to droplet impingement behavior at SLD conditions are currently limited in availability due to the relatively recent confirmation of SLD droplet existence.

The proposed model presents a significant improvement over the original formulation of DROP3D as well as the current formulation of LEWICE. The conception of a body force equivalent source term accounting for the effects of droplet–wall interactions in the equations governing droplet momentum facilitates a continued exploitation of the advantages associated with an Eulerian formulation. Hence, modeling requirements imposed by future Federal Aviation Administration certification regulations regarding the physically representative simulation of droplet impingement in the SLD regime of aircraft in-flight icing may be satisfied by the improved mathematical formulation of DROP3D.

Acknowledgments

Raimund Honsek would like to acknowledge the generous financial support of the National Sciences and Engineering Research Council of Canada in the form of an NSERC postgraduate studies scholarship, as well as a research grant provided under the NSERC-J. Armand Bombardier Chair in Multidisciplinary Computational Fluid Dynamics.

References

[1] Bragg, M. B., "Aircraft Aerodynamic Effects Due to Large Droplet Ice Accretions," AIAA Paper 96-0932, 1996.

[2] Brahimi, M. T., Tran, P., Chocron, D., Tezok, F., and Paraschivoiu, I., "Effects of Supercooled Large Droplets on Ice Accretion Characteristics," AIAA Paper 97-0306, 1997.

[3] Bourgault, Y., Habashi, W. G., Dompierre, J., and Baruzzi, G. S., "A Finite Element Method Study of Eulerian Droplets Impingement Models," *International Journal for Numerical Methods in Fluids*, Vol. 29, No. 4, May 1999, pp. 429–449. doi:10.1002/(SICI)1097-0363(19990228)29:4<429::AID-FLD795>3.0.CO;2-F

[4] Brahimi, M. T., Tran, P., Chocron, D., Tezok, F., and Paraschivoiu, I., "Effect of Supercooled Large Droplets on Ice Accretion Characteristics," AIAA Paper 97-0306, 1997.

[5] Tan, S. C., and Papadakis, M., "General Effects of Large Droplet Dynamics on Ice Accretion Modeling," AIAA Paper 2003-0392, 2003.

[6] Wright, W. B., and Potapczuk, M. G., "Computational Simulation of Large Droplet Icing," *Proceedings of the FAA International Conference on Aircraft In-Flight Icing*, Federal Aviation Administration, Washington, D.C., 1996, pp. 545–555.

[7] Rutkowski, A., Wright, W. B., and Potapczuk, M. G., "Numerical Study of Droplet Splashing and Re-Impingement," AIAA Paper 2003-0388, 2003.

[8] Bourgault, Y., Boutanios, Z., and Habashi, W. G., "Three-Dimensional Eulerian Approach to Droplet Impingement Simulation Using FENSAP-ICE, Part 1: Model, Algorithm and Validation," *Journal of Aircraft*, Vol. 37, No. 1, 2000, pp. 95–103.

[9] Morency, F., Beaugendre, H., and Habashi, W., "FENSAP-ICE, A Navier–Stokes Eulerian Droplet Impingement Approach for High-Lift Devices," *8th Aerodynamics Symposium of the Canadian Aeronautics and Space Institute*, 2001.

[10] Morency, F., Beaugendre, H., Baruzzi, G. S., and Habashi, W. G., "FENSAP-ICE: Comprehensive 3D Simulation System for In-Flight Icing," AIAA Paper 2001-2566, 2001.

[11] Hedde, T., "Modélisation Tridimensionnelle des Dépôts de Givre sur les Voilures d'Aéronefs," Ph.D. Thesis, Université Blaise-Pascal, Clermont-Ferrand, France, 1992.

[12] Ruff, G. A., and Berkowitz, B. M., "Users Manual for the NASA Lewis Ice Accretion Prediction Code (LEWICE)," NASA, Contractor Report 185129, 1990.

[13] Khan, A. R., and Richardson, J. F., "The Resistance to Motion of a Solid Sphere in a Fluid," *Chemical Engineering Communications*, Vol. 62, 1987, pp. 135–150. doi:10.1080/00986448708912056

[14] Clift, R., Grace, J. R., and Weber, M. E., *Bubbles, Drops and Particles*, Academic Press, New York, 1978.

[15] Pilch, M., and Erdman, C. A., "Use of Breakup Time Data and Velocity History Data to Predict the Maximum Size of Stable Fragments for Acceleration-Induced Breakup of a Liquid Drop," *International Journal of Multiphase Flow*, Vol. 13, No. 6, 1987, pp. 741–757. doi:10.1016/0301-9322(87)90063-2

[16] Bai, C., and Gosman, A. D., "Development of Methodology for Spray Impingement Simulation," SAE, TR 950283, 1995.

[17] Trujillo, M. F., Mathews, W. S., Lee, C. F., and Peters, J. E., "Modeling and Experiment of Impingement and Atomization of a Liquid Spray on a Wall," *International Journal of Engine Research*, Vol. 1, No. 1, 2000, pp. 87–105.

[18] Mundo, C., Sommerfeld., M., and Tropea, C., "Droplet-Wall Collisions: Experimental Studies of the Deformation and Breakup Process," *International Journal of Multiphase Flow*, Vol. 21, No. 2, 1995, pp. 151. doi:10.1016/0301-9322(94)00069-V

[19] Stow, C. D., and Stainer, R. D., "The Physical Products of a Splashing Water Drop," *Journal of the Meteorological Society of Japan*, Vol. 55, No. 5, 1977, pp. 518–532.

[20] Yarin, A. L., and Weiss, D. A., "Impact of Drops on Solid Surfaces: Self-Similar Capillary Waves and Splashing as a New Type of Kinematic Discontinuity," *Journal of Fluid Mechanics*, Vol. 283, 1995, pp. 141–173. doi:10.1017/S0022112095002266

[21] Lodej, B., "Étude et Implémentation des Phénomènes d'Éclatement de Gouttes d'Eau dans un Écoulement Diphasique," Rapport de Stage de Fin d' Étude, Institut Scientifique Polytechnique Galilée, Paris, 2003.

[22] Papadakis, M., Rachman, A., Wong, S. C., Yeong, H. W., Hung, K. E., and Bidwell, C. S., "Water Impingement Experiments on a NACA 23012 Airfoil with Simulated Glaze Ice Shapes," AIAA Paper 2004-0565, 2004.

[23] Okumura, K., Chevy, F., Richard, D., Quéré, D., and Clanet, C., "Water Spring: A Model for Bouncing Drops," *Europhysics Letters*, Vol. 62, No. 2, 2003, pp. 237–243. doi:10.1209/epl/i2003-00340-1

[24] Papadakis, M., Hung, E. K., Vu, G. T., Yeong, H. W., Bidwell, C. S., Breer, M. D., and Bencic, T. J., "Experimental Investigation of Water Droplet Impingement on Airfoils, Finite Wings and an S-Duct Engine Inlet," NASA TM-2002-211700,2002.

[25] Wright, W. B., and Potapczuk, M. G., "Semi-Empirical Modeling of SLD Physics," AIAA Paper 2004-0412, 2004.